Pharm Res (2013) 30:478–488
DOI 10.1007/s11095-012-0893-3

RESEARCH PAPER

Pharmaceutical Differences Between Block Copolymer Self-Assembled and Cross-Linked Nanoassemblies as Carriers for Tunable Drug Release

Hyun Jin Lee • Younsoo Bae

Received: 9 August 2012 / Accepted: 24 September 2012 / Published online: 9 October 2012

ABSTRACT

Purpose To identify the effects of cross-linkers and drug-binding linkers on physicochemical and biological properties of polymer nanoassembly drug carriers.

Methods Four types of polymer nanoassemblies were synthesized from poly(ethylene glycol)-poly(aspartate) [PEG-p(Asp)] block copolymers: self-assembled nanoassemblies (SNAs) and cross-linked nanoassemblies (CNAs) to each of which an anti-cancer drug doxorubicin (DOX) was loaded by either physical entrapment or chemical conjugation (through acid-sensitive hydrazone linkers).

Results Drug loading in nanoassemblies was 27~56% by weight. The particle size of SNA changed after drug and drug-binding linker entrapment (20~100 nm), whereas CNAs remained 30~40 nm. Drug release rates were fine-tunable by using amide cross-linkers and hydrazone drug-binding linkers in combination. *In vitro* cytotoxicity assays using a human lung cancer A549 cell line revealed that DOX-loaded nanoassemblies were equally potent as free DOX with a wide range of drug release half-life ($t_{1/2}$=3.24~18.48 h, at pH 5.0), but 5 times less effective when $t_{1/2}$=44.52 h.

Conclusion Nanoassemblies that incorporate cross-linkers and drug-binding linkers in combination have pharmaceutical advantages such as uniform particle size, physicochemical stability, fine-tunable drug release rates, and maximum cytotoxicity of entrapped drug payloads.

KEY WORDS cross-linked nanoassemblies · drug carriers · drug delivery · nanoparticles · polymer micelles

H. J. Lee · Y. Bae (✉)
Department of Pharmaceutical Sciences, College of Pharmacy
University of Kentucky
789 South Limestone
Lexington, Kentucky 40536, USA
e-mail: younsoo.bae@uky.edu

INTRODUCTION

Biocompatible nanoparticles, typically 10~200 nanometers (nm) in diameter, have garnered increasing attention as drug carriers in recent biomedical applications (1–3). Nanoparticles can circulate through blood vessels and accumulate preferentially in disease tissues that enhance permeation and retention of large molecules (> 1,000 atoms), such as inflammatory tissues and cancerous tumors (4–7). One important property of these nanoparticle drug carriers is capability to control drug release rates, by time or in response to stimuli (8,9), and thus maintaining drug concentrations at therapeutic dose levels in targeted sites *in vivo* to maximize therapeutic efficacy and minimize toxicity (10,11). Drug release rates, however, are still difficult to control precisely *in vivo* partially because drug carriers often change particle size, stability, biocompatibility and other physicochemical properties, which affect their drug release patterns and result in undesirable plasma protein adsorption, macrophagic uptake, and non-specific tissue distribution (12,13). Therefore, it is important to develop an easy and efficient method to fine-tune drug release rates *in vivo* for nanoparticle drug carriers.

Drug release rates are generally controlled by drug molecule diffusion and drug carrier erosion (14–16). Nanoscale drug carriers have relatively small volume to entrap drug payloads in comparison to larger drug delivery platforms (e.g. film, patches, matrices, and micro particles), leading to the development of various drug carriers that have degradable core, shell, or drug-binding linkers. Although there are many bottom-up and top-down approaches to engineer the properties of nanomaterials, one of the widely used methods to prepare nanoscale drug carriers is to exploit the self-assembling phenomenon between amphiphilic block polymers. For example, block copolymers that possess hydrophilic and hydrophobic segments form micellar

nanoassemblies, referred to as polymer micelles, providing a hydrophobic nano-compartment enveloped with a hydrophilic protection shield in aqueous solutions (17). The polymer micelles have been used in several clinical applications for the delivery of various biomedical materials, including anticancer drugs, therapeutic proteins, plasmid DNA, siRNA, contrast agents, and fluorescence probes (18). Nevertheless, polymer micelles and other supramolecular assemblies (e.g. self-assembled vesicles, lamellar, or layers) have innate limitations of particle stability in diluted conditions as they dissociate below critical micelle concentrations or the Krafft temperature (19–21). Despite these limitations, self-assemblies still have pharmaceutical advantages mainly due to their easy preparation method to design formulations for various therapeutic agents (22,23). To improve stability, molecular self-assemblies are often cross-linked in the core and shell (24–27). However, pharmaceutical differences between self-assembled and cross-linked nanoassemblies are not fully understood.

We have studied functional polymer micelles from self-assembling block copolymers, which can fine-tune drug release patterns (28–30). Our previous results demonstrate that both fast and slow drug release rates can be equally effective to suppress cancer cell growth, suggesting that drug release rates and total drug payload concentrations cannot be simply used to predict cytotoxicity of drug carriers (31–33). We hypothesized that drug carriers will achieve the maximum cytotoxicity by synchronizing drug release and cell growth rates, potentially providing a better measure to determine optimal drug release rates. This hypothesis is formulated based on the fact that most anticancer drugs are designed to kill fast-growing cells (34,35), and that drug carriers with varied drug release rates do not always show the same cytotoxicity *in vitro* and therapeutic efficacy *in vivo* (36–38). Results from previous literatures also support this hypothesis, addressing that low-dose metronomic chemotherapy appeared highly effective *in vivo*, and that cell cycle control would be a promising strategy to maximize drug efficacy to kill cancer cells (39,40). Although these facts emphasize the pharmaceutical importance of drug release rates on therapeutic efficacy of drug carriers, most existing drug carriers are developed mainly by focusing to increase total drug concentrations in tumors and inside cells, while the effects of drug release rates on cytotoxicity remains unclear as drug carriers can interact directly with cells and alter cell viability. For example, some polymer surfactants destabilize the cellular membrane, either increasing intracellular drug concentrations or breaking down the cells to death (41–43). Therefore, drug carriers should be non-toxic to investigate the effect of drug release rate on cytotoxicity more accurately.

For these reasons, we selected biocompatible poly(ethylene glycol)-poly(aspartate) [PEG-p(Asp)] block copolymers, which we have been using in previous studies and confirmed safety *in vitro* and *in vivo* (44–47). PEG is a biocompatible polymer used widely in biomedical applications for surface coating to avoid agglomeration, protein adsorption, and the immune response of materials *in vivo*, and drug carriers modified with PEG have shown to enhance blood circulation time and reduce toxicity and immune response (48). In addition to biocompatibility, particle size and shape were previously identified as factors that change intracellular uptake and *in vivo* distribution of drug carriers (49,50), indicating that 30 ~ 150 nm particles can accumulate in tumor tissues most effectively (51,52). As for a drug payload, an anticancer drug doxorubicin (DOX) was used in this study because DOX, alone or in combination with other drugs, is frequently used for the treatment of various cancers in clinic (53,54). In addition, DOX has strong UV-Visible absorption and fluorescence, which are beneficial for easy drug quantification. We previously confirmed that DOX is a model anticancer drug suitable for drug delivery studies because it remains chemically and biologically active during the processes of its entrapment to and release from drug carriers (28).

To test our hypothesis and rationally design a more effective drug carrier, we prepared four types of nanoassemblies as model nanoparticle drug carriers with similar biocompatibility (surface-modified with PEG), particle size (<100 nm), and drug entrapment yields (> 10 weight %). These nanoassemblies were designed to control drug release rates by using drug-binding and cross-linkers in combination (Fig. 1). The first type of a nanoassembly is a block copolymer self-assembled nanoassembly, dubbed SNA, which is a polymer micelle prepared from PEG-p(Asp) block copolymers in the presence of Ca^{2+} ions as well as DOX (31). The second nanoassembly, Hyd-SNA, is SNA to which DOX was conjugated through a hydrazide drug-binding linker, which we previously showed to form an acid-labile hydrazone bonding with DOX (30,55). The third nanoassembly is a cross-linked nanoassembly (CNA), which is SNA cross-linked in the core with amide bonds (44). Lastly, the fourth nanoassembly, Hyd-CNA, is a nanoassembly newly prepared for this study by crosslinking Hyd-SNAs and incorporating hydrazide drug-binding linkers in the core in combination. DOX was entrapped through either physical entrapment to SNA and CNA, or covalent chemical conjugation to Hyd-SNA and Hyd-CNA, respectively. These four types of nanoassemblies were characterized as detailed below to study their physicochemical and biological properties *in vitro*. Results from this study, therefore, provide a better understanding of pharmaceutical differences between self-assembled and cross-linked nanoassemblies.

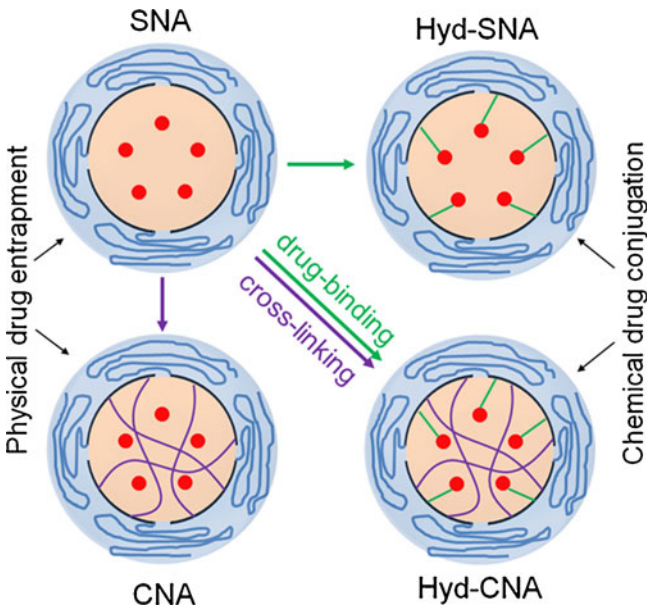

Fig. 1 Nanoassemblies used in this study. Biocompatible poly(ethylene glycol)-poly(aspartate) block copolymers were modified with drug binding linkers (green arrow) and cross-linkers (purple arrow) in combination to prepare 1) miellar block copolymer self-assembling nanoassemblies (SNA); 2) SNA with hydrazide drug binding linkers (Hyd-SNA); 3) cross-linked nanoassembly (CNA); and 4) CNA with drug-binding linkers (Hyd-CNA). SNA and CNA entrapped an anticancer drug doxorubicin (DOX) through physical entrapment while Hyd-SNA and Hyd-CNA loaded DOX through acid-labile hydrazone conjugation.

MATERIALS AND METHODS

Chemicals and Cell Line

L-Aspartic acid β-benzyl ester (BLA), triphosgene, anhydrous hydrazine, N,N′-diisopropylcarbodiimide (DIC), N-hydroxysuccinimide (NHS), adipic acid, triethylamine, dimethylsulfoxide-*d6* (DMSO-*d6*), anhydrous tetrahydrofuran (THF), anhydrous hexane, anhydrous dimethylsulfoxide (DMSO), anhydrous ethyl ether, benzene, acetate buffer solutions (pH 5.0, 10 mM), phosphate buffer solutions (pH 7.4, 10 mM), and doxorubicin hydrochloride (DOX) were purchased from Sigma-Aldrich (USA). α-Methoxy-ω-amino poly(ethylene glycol) (PEG or mPEG-NH_2) with 5 kDa molecular weight (MW) was purchased from NOF Corporation (Japan). Calcium chloride, regenerated cellulose dialysis bags with molecular weight cut off (MWCO) 6~8 kDa and 50 kDa, Slide-A-Lyzer® G2 dialysis cassettes with MWCO 10 kDa, and Sephadex LH-20 gels were purchased from Fisher Scientific (USA). Amicon-Ultra centrifugal ultrafiltration devices with MWCO 100 kDa were purchased from Millipore (USA). A human non-small cell lung cancer A549 cell line and F12K cell culture medium were obtained from ATCC (USA). Fetal bovine serum (FBS) and phosphate buffered saline (PBS) were provided by Atlanta Biologicals (USA).

Block Copolymer Synthesis

Our synthesis protocol is summarized in Fig. 2. β-Benzyl-L-aspartate N-carboxy anhydride (BLA-NCA, 3) was synthesized as a monomer by the Fuchs-Farthing method as previously reported (56). Briefly, BLA, 1, was reacted with 1.3 fold triphosgene, 2, in dry THF under nitrogen atmosphere at 45°C, 100 mg/mL, until the solution became clear. Anhydrous hexane was slowly added to the solution until NCA crystals appeared and disappeared quickly. The solution was recrystallized at −20°C overnight. Needle-like BLA-NCA crystals were washed with anhydrous hexane and dried under vacuum for the block copolymer synthesis.

Ring-opening polymerization of BLA-NCA was conducted by using mPEG-NH_2, 4, as a macroinitiator to prepare poly(ethylene glycol)-poly(β-benzyl L-aspartate) (PEG-PBLA, 5) block copolymers. The polymerization reaction was carried out in anhydrous DMSO at 45°C for 2 days. PEG-PBLA was precipitated in anhydrous ethyl ether, and freeze-dried from benzene.

PEG-p(Asp), 6, was prepared by deprotecting benzyl groups from PEG-PBLA in 0.1 N NaOH solution. PEG-p(Asp) in a deionized form was also prepared by removing Na salts through the dialysis of the polymer in 0.1 M HCl solution and subsequently deionized water. PEG-p(Asp) block copolymers in sodium salt and free carboxylate forms were collected by freeze drying.

The benzyl esters of PEG-PBLA block copolymers were replaced with hydrazide (Hyd) through aminolysis reaction to obtain PEG-p(Asp-Hyd), 7, block copolymers as reported previously (57). Excess hydrazine, 10 fold with respect to the number of BLA repeating units, was reacted with PEG-PBLA in DMSO at 40°C, 50~100 mg/mL, for 1 h. Polymer products were purified through repetitive ether precipitation, dialysis against deionized water (MWCO 6~8 kDa), and collected by freeze-drying.

Preparation of Particles Entrapping DOX

We synthesized four types of DOX-loaded particles in this study. Synthesis steps are shown also in Fig. 2 while the particle structures are illustrated in Fig. 1.

SNA, 8, was synthesized by mixing sodium salt PEG-p(Asp) block copolymers with DOX in deionized water as we reported previously (31). The polymer concentration was 10 mg/mL, while DOX was added at 1:1 molar ratio with respect to carboxyl groups of PEG-p(Asp). Calcium chloride, 9, was used as a salt bridge between the block copolymer and DOX to stabilize the drug-loaded nanoassemblies. SNA was dialyzed against deionized water using MWCO 50 kDa, followed by ultrafiltration with MWCO 100 kDa to remove DOX bound weakly on the particle. SNA was freeze-dried, reconstituted in

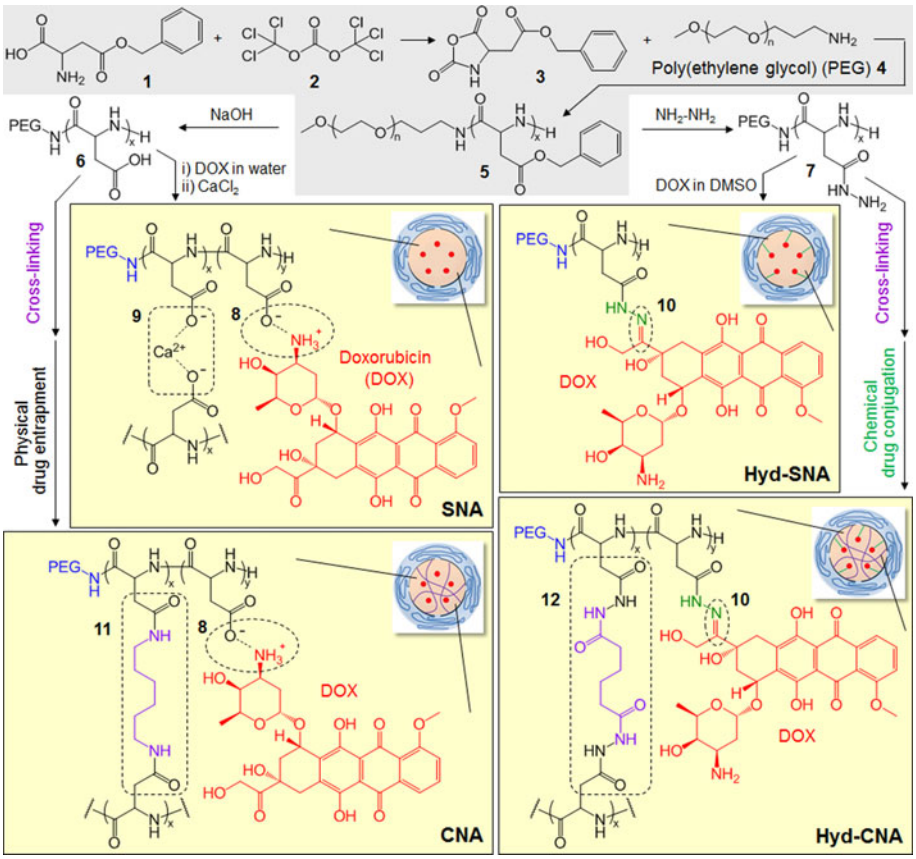

Fig. 2 Synthesis of block copolymers and nanoassemblies. The same batch of block copolymer (5 in a gray box) was used to prepare all nanoassemblies (SNA, Hyd-SNA, CNA, and Hyd-CNA in yellow boxes), following the procedures of side chain modification, cross-linking and drug binding as shown in arrows. The dashed circles indicate the binding sites of DOX (desalted), which were used for drug conjugation through either an ionic interaction or a hydrazone bond between the drug and anionic block copolymers. The dashed rounded rectangles indicate the formation of a calcium salt bridge or amide cross-liking between block copolymer chains.

deionized water, and filtered through 0.22 μm filters prior to determining its particle size and drug loading.

Hyd-SNA, 10, was synthesized by two steps. First step was to conjugate DOX, desalted with triethylamine, to the hydrazide groups of PEG-p(Asp-Hyd) in DMSO with a 1:1 molar ratio at 30°C, 50 mg/mL, for 2 days, while the drug-conjugated polymers were purified by ether precipitation and Sephadex LH20 gel separation, followed by freeze drying. In next step, the drug-polymer conjugates were dissolved in DMSO and titrated in deionized water to form micelles. The micelles were dialyzed using a MWCO 50 kDa membrane, purified further by ultrafiltration (MWCO 100 kDa), and freeze-dried, producing Hyd-SNA. The final product was reconstituted in water and sterilized by 0.22 μm filtration.

CNA, 11, was prepared by cross-linking PEG-p(Asp) through an amide coupling reaction. Carboxyl groups of PEG-p(Asp) were reacted with 1,8-diaminooctane at 1:1 molar ratio in the presence of DIC, NHS, and DMAP (2:2:0.2 fold) in DMSO at room temperature for 3 days. The cross-linked PEG-p(Asp) was dialyzed against DMSO and then water with MWCO 50 kDa, followed by ultrafiltration (MWCO 100 kDa) and lyophilization to collect empty CNA powder. DOX and empty CNA were mixed at an equivalent molar ratio in deionized water, and purified following the steps used for SNA, 8. No calcium ions were used for CNA.

Hyd-CNA, 12, was prepared by cross-linking PEG-p(Asp-Hyd) through amidation reaction. Adipic acid was used as a cross-linker between PEG-p(Asp-Hyd) block copolymers. The cross-linking reaction was conducted in DMSO at room temperature for 3 days by adjusting the molar ratio adipic acid and the hydrazide groups of PEG-p(Asp-Hyd) to fine-tune cross-linking yields, while DIC, NHS, and DMAP were used as coupling reagent as used for aforementioned CNA synthesis. Cross-linked PEG-p(Asp-Hyd) block copolymers were purified by dialysis against DMSO and ether precipitation, and subsequently mixed with desalted DOX in DMSO at 50 mg/mL for drug conjugation at 30°C for 2 days. DOX was entrapped in Hyd-CNA as similar to Hyd-SNA, 10. The final product, Hyd-CNA, was filter-sterilized (0.22 μm), following precipitation in ethyl ether, gel separation, and freeze drying.

Material Characterization

Proton nuclear magnetic resonance (^{1}H-NMR, Varian, 400 MHz) measurements were used to determine the compositions of block copolymers and nanoassemblies in DMSO-*d6* and D_2O, respectively. The number average molecular weights (Mn) of block copolymers and nanoassemblies were calculated by gel permeation chromatography (GPC, Shimadzu LC20, Japan) equipped with RI and UV detectors, using PEG

standard and a phosphate buffered saline (PBS, 1X) mobile phase. Particle sizes of nanoassemblies were determined by dynamic light scattering (DLS, Zetasizer Nano 90, Malvern, UK) measurements at a 173° fixed angle. All samples were prepared in aqueous solutions at 2 mg/mL and filtered through 0.22 μm filters prior to GPC and DLS analyses. DOX loading and release were quantified using ultraviolet-visible spectrophotometry spectroscopy (UV-Vis, absorbance at 480 nm, SpectraMax M5, Molecular Devices, USA).

Drug Release Experiment

All particles entrapping DOX were dissolved in deionized water (0.5 mg/mL), and transferred to six dialysis cassettes (MWCO 10 kDa). A group of three dialysis cassettes was used for each sample, and placed in an either pH 5.0 or pH 7.4 buffer solution (20 mM). Drug release patterns were monitored under the sink condition as the volume of dialysis medium was maintained 3,000 times greater (5 L) than the volume of the sample solution in the dialysis cassettes (1.65 mL/cassette, $n=3$). Sample solutions were dialyzed at 37°C for 48 h. DOX remaining in each dialysis cassette was measured at 0, 1, 3, 6, 10, 24, 34, and 48 h. Data were converted to DOX released with respect to the initial DOX amount.

Cytotoxicity Assay

A human non-small cell lung cancer A549 cell line was used to determine the cytotoxicity of empty nanoassemblies, DOX-loaded nanoassemblies, and free DOX. Cells were seeded in a 96-well plate (5,000 cells/well) in 100 μL F12K cell culture medium containing 10% FBS. After 24 hours, serial dilutions of the samples were added to the cell plate. Cells were then incubated at 37°C, 5% CO_2, for 72 hours, followed by cell viability measurement using a resazurin assay that indicates mitochondrial metabolic activity in live cells. Resazurin solution in PBS (10 μL, 1 mM) was added to the sample-treated cells at the end of the 72-hour treatment period. Three hours later, the fluorescence of resorufin, metabolited resazurin, was measured at 560 nm (excitation)/590 nm (emission). The half maximal inhibitory concentration (IC50) was calculated with Prism software (GraphPad, USA).

Statistics

Data are expressed means±standard deviation (SD) from triplicate experiments unless mentioned otherwise. Statistical differences were determined by one-way analysis of variance (ANOVA) analysis. A difference was considered statistically significant when $p<0.05$, and denoted by an asterisk symbol (*).

RESULTS

Polymer Synthesis

PEG-p(Asp) and PEG-p(Asp-Hyd) block copolymers were obtained from PEG-PBLA as previously reported (45). ^{1}H-NMR determined that PEG-PBLA block copolymer (5 in Fig. 2) consisted of a PEG chain (Mn=5,000) and 33 aspartate repeating units, which was determined by integrating PEG (3.5 ppm) and benzyl (7.3 ppm) peaks. The block copolymer composition is denoted as 5-33, where the two numbers indicate the molecular weight of PEG$\times 10^{-3}$ and the number of repeating aspartate units, respectively. PEG-p(Asp) showed a single peak with a narrow distribution (polydispersity index (PDI)<1.2), which was eluted before 5 kDa PEG used as an initiator, indicating successful polymer synthesis and absence of homopolymers. PEG-p(Asp-Hyd) also showed a narrow molecular weight distribution. Therefore, PEG-PBLA, PEG-p(Asp), and PEG-p(Asp-Hyd) block copolymers showed purity as we confirmed previously.

Nanoparticle Preparation

SNA, Hyd-SNA, CNA, and Hyd-CNA nanoassemblies (Fig. 1) were characterized first by GPC, which showed a single peak with molecular weight of 140~160 kDa for CNA and Hyd-CNA and 200~250 kDa for SNA and Hyd-SNA. These molecular weights are relative values as calculated from a calibration curve prepared using PEG standard and a GPC column with a size exclusion limit of 3×10^6 Da. Although the absolute molecular weight for each particle could not be determined, a single GPC peak indicates that nanoassemblies are homogeneous (data not shown). In particular, CNA and Hyd-CNA showed extremely narrow PDI (< 1.15).

Particle sizes of nanoassemblies were subsequently determined by DLS. All particles were smaller than 60 nm before entrapping DOX (Fig. 3). However, SNA and Hyd-SNA, which are self-assembled nanoassemblies, increased the particle size after DOX entrapment. On the contrary, CNA and Hyd-CNA showed no statistically significant changes before and after loading DOX, and the particle sizes of these cross-linked nanoassemblies were smaller than 40 nm regardless of drug entrapment approaches (physical entrapment *versus* chemical conjugation). As for drug entrapment, SNA showed the highest DOX loading by 56 weight % (wt%), followed by Hyd-SNA (42 wt%), Hyd-CNA (37 wt %), and CNA (27 wt%). Despite the different particle size and drug entrapment yield, none of the particles showed agglomeration or precipitation in water.

DOX-loaded nanoassemblies with a cross-linked core (CNA and Hyd-CNA) enhanced particle stability during purification and storage in comparison to SNA and Hyd-SNA that interacted with ultrafiltration membrane when

highly concentrated (> 100 mg/mL) forming gel-like materials. No precipitation was observed under normal conditions handling nanoparticle solutions at concentrations lower than 20 mg/mL. Nanoassemblies readily went through 0.22 μm filters, and could be reconstituted in aqueous solutions (e.g. deionized water) after freeze drying. Despite enhanced particle stability and easy sterilization, we stored nanoassemblies as powder and prepared fresh samples for every experiment to avoid variability in quality of samples between batches. DOX concentrations were determined using filter-sterilized nanoassemblies.

Drug Release Rates

Figure 4 shows DOX release patterns for SNA, Hyd-SNA, CNA, and Hyd-CNA. The determination of drug release half-life ($t_{1/2}$) at the physiological condition pH 7.4 was problematic because Hyd-CNA released drugs less than 50% in 48 hours. In addition, CNA released drugs quickly at pH 7.4, expanding the $t_{1/2}$ range too broad to compare the effect of drug release rates on cytotoxicity of different nanoassemblies. All polymer nanoassemblies accelerated DOX release at pH 5.0 in comparison to pH 7.4, releasing more than 50% of drug entrapped in 48 hours. Our preliminary experiments showed that cell division time (t_{div}) for A549 cells was average 22 hours. Therefore, we calculated $t_{1/2}$ at pH 5.0 rather than 7.4, which allowed us to determine $t_{1/2}$ for all nanoassemblies within 48 hours while comparing conditions of $t_{1/2} < t_{div}$ and $t_{1/2} > t_{div}$ (denoted as Groups 1 and 2 in Table I). Determining $t_{1/2}$ at pH 5.0 is also clinically relevant because intracellular lysosomes (pH 4.8) and endosomes (pH 5.5 ~ 6.5) are acidic (58).

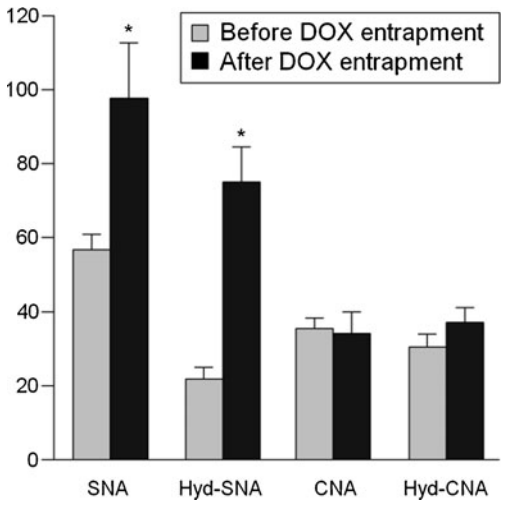

Fig. 3 Particle size changes of nanoassemblies before and after drug entrapment. Dynamic light scattering (DLS) was used to determine the average particle size and distribution of nanoassemblies in deionized water. The asterisks indicate a significant difference in the particle size between empty and drug-loaded nanoassemblies ($p < 0.05$).

Accumulated amount of drugs released from nanoassemblies was also compared at pH 7.4 and 5.0 for 48 hours for each nanoparticle. As shown in Table I, only nanoassemblies entrapping through covalent drug conjugation (Hyd-SNA and Hyd-CNA) showed a significant difference in acid-accelerated drug release, releasing approximately 24 ~ 27% more drugs at pH 5.0 as opposed to pH 7.4, whereas the total drugs released from SNA and CNA (DOX was entrapped through physical entrapment) appeared similar. Interestingly, SNA released 98% of total DOX entrapped, yet CNA, released drugs at the fastest rate regardless of pHs, still entrapped 11 ~ 20% of DOX inside the particle. We confirmed that free DOX escaped completely from the dialysis bags in a few hours, and thus, 2% drugs in SNA as well as 11 ~ 20% DOX in CNA were considered being entrapped not in the dialysis bag but inside nanoassemblies.

Cytotoxicity

Biological activity of drug-loaded nanoassemblies was then evaluated by *in vitro* cytotoxicity assays, using free DOX and empty nanoassemblies as controls (Table I and Fig. 5). The cytotoxicity assays revealed that faster drug release did not always lead to greater cytotoxicity of nanoassemblies. CNA, which showed the shortest drug release half-life, was as potent as free DOX and SNA in terms of IC50 values (Table I). SNA released drugs approximately 50% slower than CNA, $t_{1/2}$=6.37 *versus* 3.24 hours (Fig. 4a, c), yet it was also similarly effective to kill A549 cancer cells compared with free DOX. As $t_{1/2}$ becomes longer, nanoassemblies showed a lower IC50 value, and Hyd-SNA ($t_{1/2}$=18.38 h) was 2.2 fold less potent than CNA ($t_{1/2}$=3.24 h) based on IC50 values. Interestingly, our data demonstrate that the drug release rate ($t_{1/2}$) is not linearly proportional to cytotoxicity (IC50), but instead, $t_{1/2}$ needs to be shorter than cell division time (t_{div}) for nanoassemblies to kill cancer cells effectively. It is noted that Hyd-CNA ($t_{1/2}$=44.52 and 51.50% drug released) showed the highest IC50 value (2.65 μM or 5 times less active than free DOX), considering that t_{div} of A549 cells was 22 hours and that Hyd-CNA has similar drug release half-life and drug release efficiency compared to Hyd-SNA. Figure 5 shows dose-response curves of nanoassemblies with and without DOX, indicating that toxicity of empty drug carriers is negligible. These results suggest that the drug release rate might be the rate-determining factor for cytotoxicity of nanoassemblies because other particle properties such as particle size (<100 nm), stability (no precipitation over time), and surface properties (PEG coating) were similar among nanoassemblies. It is also surmised that fine-tuning of drug release with respect to cell division time could maximize drug efficacy by using drug molecules efficiently.

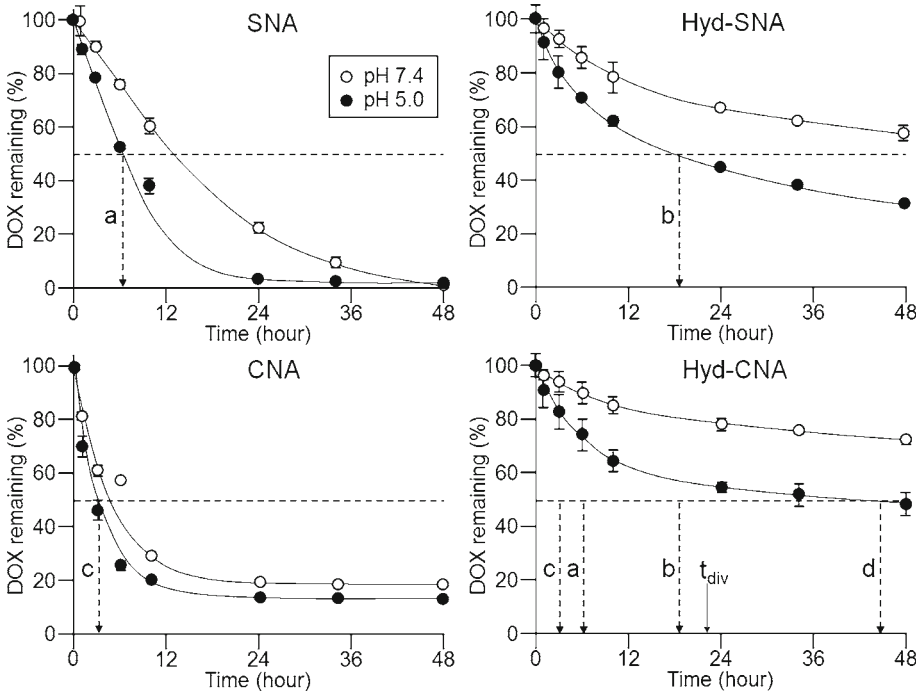

Fig. 4 Drug release-time curves for nanoassemblies. Drug release patterns were determined for 48 hours at pHs 7.4 and 5.0, corresponding to the physiological and lysosomal conditions respectively. Drug release half-life ($t_{1/2}$=a, b, c, and d) was determined by curve-fitting for each nanoparticle at pH 5.0. Cell division time (t_{div}=22 h) was determined from preliminary experiments for a human non-small lung cancer A549 cell line.

DISCUSSION

Fast drug release is commonly expected to lead to greater drug efficacy for drug carriers. Such common expectation, however, does not explain how drug carriers can be equally, or even more, potent in comparison to free drug formulations *in vivo* (28,59). Enhanced drug delivery to tumors and improved bioavailability of drug are two major factors that also frequently explain greater therapeutic efficacy and low toxicity of drug-loaded drug carriers as opposed to free drugs (60,61). However, no drug carriers show the same therapeutic efficacy *in vivo*, even if the same drug payload was used (62,63). We also confirmed significant differences in *in vivo* antitumor activity and toxicity profiles of drug carriers, which can control drug release in response to *in vivo* stimuli or cell-specific receptors (47,55,64). Previous studies also pointed out that particle size, shape, and surface charge can be important as well to determine *in vivo* performance of drug carriers (65–67). Nevertheless, the answers to these questions remained difficult because each drug carrier employs a different approach to control drug release patterns, which affects aforementioned particle properties.

In this study, therefore, we prepared four types of particles, which have drug-binding linkers and cross-linkers in combination, by using self-assembling block copolymer micelles as a

Table I Summary of Data Analyzed

Samples	Control	Nanoassemblies[a]			
	Free DOX	Group 1		Group 2	
		SNA	Hyd-SNA	CNA	Hyd-CNA
Drug release half-life, $t_{1/2}$, (hour)[b]	N/A	6.37	18.48	3.24	44.52
Accumulated drug release at pH 7.4 in 48 h (%)[c]	100	99.14	42.49	80.26	27.90
Accumulated drug release at pH 5.0 in 48 h (%)[c]	100	98.28	69.10	89.27	51.50
IC 50 (μM, DOX equivalent)	0.53 ± 0.20	0.64 ± 0.57	0.86 ± 0.35	0.39 ± 0.08	2.65 ± 1.04
Relative cytotoxicity	1.00	1.21	1.62[d,*]	0.74	5.00 [e,*]

[a] Nanoassemblies were divided based on the drug release half-life ($t_{1/2}$) and cell division time (t_{div}): Group 1 ($t_{1/2} < t_{div}$) and Group 2 ($t_{1/2} > t_{div}$)

[b] Drug release half-life was determined by plotting drug release-time curves in Fig. 4

[c] Accumulated drug release was calculated from area under the drug release-time curve (AUC) in Fig. 4, and normalized with respect to the initial drug loading (100%)

[d] Data were significantly different in comparison to CNA

[e] Data were significantly different in comparison to Free DOX

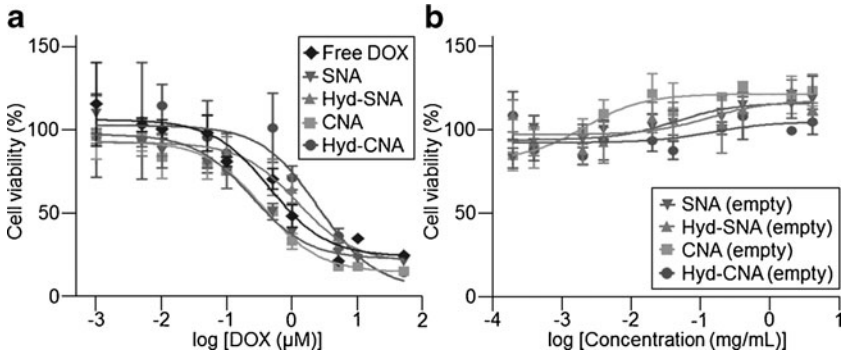

Fig. 5 Dose-response curves for drug-loaded nanoassemblies. Cell viability was determined by exposing A549 cells to the serial dilutions of free DOX, empty nanoassemblies, and DOX-loaded nanoassemblies. (**a**) All sample concentrations were based on free DOX concentrations. (**b**) Toxicity of empty nanoassemblies was evaluated by polymer concentrations, covering the range of polymer mass required for drug-loaded nanoparticles with varied drug loading yields (> 27 wt%) in (**a**).

starting template (Fig. 1). These four types of particles represent: 1) nanoparticle drug carriers coated with biocompatible PEG and loaded with anticancer drugs through physical entrapment (SNA); 2) nanoassemblies similar to SNA but entrapping drugs through a pH-labile linker that degrades in either extracellular tumoral or intracellular acidic condition (Hyd-SNA); 3) nanoassemblies based on SNA and cross-linked in the core for improved particle stability (CNA); and 4) nanoassemblies with improved particle stability and controlled drug release capability (Hyd-CNA). These particles were successfully prepared by synthesis protocols (Fig. 2) as previous reported with slight modification.

Particle sizes of empty nanoassemblies were similar, ranging between 20~60 nm (Fig. 3). Drug entrapment led to a considerable change in particle size, while SNA and Hyd-SNA doubled and tripled the particle size respectively. Considering that these two nanoassemblies are formed from self-assembling block copolymers, it is speculated that block copolymers rearranged during drug entrapment and produced larger particles, which are stable enough to retain spherical structure in water avoiding precipitation. SNA contained calcium salt and DOX, which would have stabilized the particles effectively, retaining particle size below 100 nm (clinically relevant to accumulate in tumors efficiently). It is likely that Hyd-SNA formed smaller particles than SNA because it has longer side chains modified with hydrazide groups that were further conjugated with drug payloads, which contributed together to form a compact core in the particle. In comparison to self-assembled particles, polymer cross-linked nanoassemblies retained particle size before and after drug entrapment. CNA, which loaded DOX through physical entrapment similarly to SNA, was as small as Hyd-CNA where DOX was conjugated through a hydrazone bond. It is noted that CNA and Hyd-CNA with cross-linked cores still showed efficient drug entrapment yield (> 27 wt %), although that was approximately 10% lower than that of SNA or Hyd-SNA. The drug entrapment yield of Hyd-CNA (37 wt%), slightly higher than CNA (27 wt%), is likely attributed to that hydrazide drug binding linkers provide more space for DOX molecules to get inside the particle. These results demonstrate that four nanoassemblies with similar particle properties are successfully prepared.

Drug release patterns of the four nanoassemblies were distinctive enough to show varied drug release half-life. Figure 4 indicates that nanoassemblies entrapping drugs through covalent chemical conjugation release drug slowly than through physical entrapment (SNA *versus* Hyd-SNA or CNA *versus* Hyd-CNA). Cross-linking led to accelerated drug release in CNA, yet slowed down drug release from Hyd-CNA. Although both CNA and Hyd-CNA were mixed with DOX after cross-linking the cores, DOX molecules may be present at the vicinity rather than the center of the cross-linked core of CNA while they are likely entrapped in the core of Hyd-CNA. This hypothesis is supported partially by an increase, even though it is subtle, in particle size of Hyd-CNA following DOX entrapment in comparison to CNA (Fig. 3). Figure 4 also shows that four types of nanoassemblies can be categorized by two nanoparticle groups according to the drug release half-life ($t_{1/2}$=a, b, c, and d) with respect to cell division time (t_{div} in Fig. 4, average 22 hours for A549 cells): 1) Group 1 with $t_{1/2}<t_{div}$ (SNA, Hyd-SNA, and CNA); and 2) Group 2 with $t_{1/2}>t_{div}$ (Hyd-CNA). Nanoassemblies, regardless of the composition, released DOX faster at pH 5.0 than pH 7.4, leading to an increase in total drug release. Nanoassemblies entrapping DOX through physical entrapment (SNA and CNA) released more than 80% of total drug in 48 hours, while Hyd-SNA and Hyd-CNA, nanoassemblies entrapping drugs through covalent chemical conjugation, led to 69.10% and 51.50% drug release at pH 5.0 in 48 hours (42.49% and 27.90% at pH 7.4), respectively.

Subsequent cell experiments revealed that fast drug release did not always result in greater cytotoxicity of nanoassemblies, evaluated by IC50 values, but that nanoassemblies with drug release half-life ($t_{1/2}$) shorter than cell division time (t_{div}) killed

cells as effective as free drugs. The IC50 values and relative cytotoxicity of the nanoassemblies are summarized in Table I, indicating that all nanoassemblies in Group 1 (SNA, Hyd-SNA, and CNA) were more effective to kill cells than Hyd-CNA (Group 2). Within in the same group, nanoassemblies that released drugs faster ($t_{1/2}$=c<a<b, Fig. 4) indeed showed lower IC50 values (IC50=c<a<b, Table I), yet their relative cytotoxicity was within 2 fold in comparison to free DOX. On the contrary, the IC50 value of Hyd-CNA was 5 fold greater than free DOX, showing less anticancer efficacy. Although data are still limited to draw a general conclusion, these results suggest that drug release rates should be synchronized with cell division time to maximize drug efficacy, which may partially explain why drug carriers that release drugs slowly *in vivo* can still show effective antitumor activity *in vivo*. At the same time, it is expected that drug carriers that release drugs in a tunable manner would be effective to shrink tumors comprising cancer cells with different cell division times (e.g. fast-growing and quiescent cancer cells affected by heterogeneous oxygen supply, blood flow, interstitial pressure, and other tumor microenvironmental factors).

Cytotoxicity of a drug-loaded drug carrier is often attributed to toxicity of the empty drug carrier, which can behave as a surfactant to destabilize the cancer cell membrane or interacts with intracellular organelles (e.g. mitochondria, transporters, and enzymes), causing the programmed cell death (apoptosis). Figure 5 confirmed that all empty nanoassemblies used in this study caused no toxicity at a concentration up to 10 mg/mL, which is clinically relevant to carry their drug payload at a therapeutic level *in vivo* (i.e. If drug loading is 10 wt%, a dose of 10 mg drug/kg can be achieved by injecting 1% drug solution with respect to a body weight of a patient as well as animal). Therefore, any additive cytotoxicity caused by nanoassemblies is negligible under experimental conditions in this study, considering the high DOX entrapment yield for each nanoparticle (SNA: 56 wt%; Hyd-SNA: 42 wt%; CNA: 27 wt%; and Hyd-CNA: 37 wt %). However, mechanisms of differential cellular responses to drug carriers with varied drug release rates should be detailed further in future studies because this study demonstrated only that fast drug release rates or high concentrations of drug released from nanoassemblies resulted in greater cytotoxicity, and furthermore, cell death is a complicated event that can be triggered by different reasons.

CONCLUSION

Four types of nanoassemblies, modified through covalent drug-binding and core cross-linking in combination, were prepared in this study to identify the differences in physicochemical and biological properties of polymer nanoassembly drug carriers. Particle properties, such as particle size (< 100 nm), drug entrapment yields (27~56 wt%), and surface property (PEG coating), were controlled similar between the nanoassemblies to avoid variables that could affect cytotoxicity. In comparison to an approach to cross-link the particle core, the covalent conjugating of drugs to nanoassemblies was a more effective way to increase the release half-life ($t_{1/2}$) for an anticancer drug (DOX), ranging between 3.24 and 44.52 h at the lysosomal condition (pH 5.0). *In vitro* cytotoxicity assays revealed that nanoassemblies (SNA, Hyd-SNA, and CNA) were equally effective as free DOX to kill cancer cells as long as the $t_{1/2}$ (3.24~18.48 h) is shorter than the cell division time (t_{div}, 22 hours for A549). On the contrary, Hyd-CNA with $t_{1/2}$=44.52 h (> t_{div}) was 5 fold less effective in killing cells compared to free DOX or other nanoassemblies. Although further studies are needed, these results suggest that optimal drug release rates for nanoparticle drug carriers can be determined by controlling the drug release half-life with respect to cell division time to maximize therapeutic efficacy of anticancer drug payloads. In conclusion, nanoassemblies to which cross-linkers and drug-binding linkers are incorporated in combination would provide pharmaceutical advantages such as uniform particle size, physicochemical stability, fine-tunable drug release rates, and maximum cytotoxicity of entrapped drug payloads.

ACKNOWLEDGMENTS AND DISCLOSURES

This research is supported by the Kentucky Lung Cancer Research Program. Authors thank Alli Eckman for assisting cytotoxicity assays.

REFERENCES

1. Farokhzad OC, Langer R. Impact of nanotechnology on drug delivery. ACS Nano. 2009;3:16–20.
2. Yokoyama M. Polymeric micelles as a new drug carrier system and their required considerations for clinical trials. Exp Opin Drug Del. 2010;7:145–58.
3. Cabral H, Kataoka K. Multifunctional nanoassemblies of block copolymers for future cancer therapy. Sci Technol Adv Mat. 2010:11
4. Victor EG, Silveira PCL, Possato JC, da Rosa GL, Munari UB, de Souza CT, Pinho RA, da Silva L, Streck EL, Paula MMS. Pulsed ultrasound associated with gold nanoparticle gel reduces oxidative stress parameters and expression of pro-inflammatory molecules in an animal model of muscle injury. J Nanobiotechnol. 2012:10
5. Bisht S, Khan MA, Bekhit M, Bai HB, Cornish T, Mizuma M, Rudek MA, Zhao M, Maitra A, Ray B, Lahiri D, Maitra A, Anders RA. A polymeric nanoparticle formulation of curcumin (NanoCurc (TM)) ameliorates CCl4-induced hepatic injury and fibrosis through reduction of pro-inflammatory cytokines and stellate cell activation. Lab Invest. 2011;91:1383–95.
6. Fang J, Qin HB, Nakamura H, Tsukigawa K, Shin T, Maeda H. Carbon monoxide, generated by heme oxygenase-1, mediates the enhanced permeability and retention effect in solid tumors. Cancer Sci. 2012;103:535–41.

7. Sancey L, Barbier E, Hirsjarvi S, Dufort S, Benoit JP, Remy C, Coll JL. Enhanced Permeability and Retention (EPR) effect in tumors: characterization by MRI and fluorescence imaging. B Cancer. 2011;98:S67.
8. Santi DV, Schneider EL, Reid R, Robinson L, Ashley GW. Predictable and tunable half-life extension of therapeutic agents by controlled chemical release from macromolecular conjugates. PNAS. 2012;109:6211–6.
9. Wei CA, Guo J, Wang CC. Dual stimuli-responsive polymeric micelles exhibiting "AND" logic gate for controlled release of adriamycin. Macromol Rapid Comm. 2011;32:451–5.
10. Fang J, Nakamura H, Maeda H. The EPR effect: Unique features of tumor blood vessels for drug delivery, factors involved, and limitations and augmentation of the effect. Adv Drug Deliv Rev. 2011;63:136–51.
11. Miyata K, Nishiyama N, Kataoka K. Rational design of smart supramolecular assemblies for gene delivery: chemical challenges in the creation of artificial viruses. Chem Soc Rev. 2012;41: 2562–74.
12. Jackson SP, Bartek J. The DNA-damage response in human biology and disease. Nature. 2009;461:1071–8.
13. Solier S, Zhang YW, Ballestrero A, Pommier Y, Zoppoli G. DNA damage response pathways and cell cycle checkpoints in colorectal cancer: current concepts and future perspectives for targeted treatment. Curr Cancer Drug Tar. 2012;12:356–71.
14. Drummond DC, Noble CO, Hayes ME, Park JW, Kirpotin DB. Pharmacokinetics and *in vivo* drug release rates in liposomal nanocarrier development. J Pharm Sci. 2008;97:4696–740.
15. Pamies P. Optimized for the clinic. Nat Mater. 2012;11:358.
16. Siepmann J, Siepmann F. Mathematical modeling of drug delivery. Int J Pharm. 2008;364:328–43.
17. Croy SR, Kwon GS. Polymeric micelles for drug delivery. Curr Pharm Des. 2006;12:4669–84.
18. Kwon GS, Forrest ML. Amphiphilic block copolymer micelles for nanoscale drug delivery. Drug Dev Res. 2006;67:15–22.
19. Beheshti N, Kjoniksen AL, Zhu KZ, Knudsen KD, Nystrom B. Viscosification in polymer-surfactant mixtures at low temperatures. J Phys Chem B. 2010;114:6273–80.
20. Lu CH, Mikhail AS, Wang XY, Brook MA, Allen C. Hydrogels containing core cross-linked block co-polymer micelles. J Biomat Sci-Polym E. 2012;23:1069–90.
21. Oberoi HS, Nukolova NV, Laquer FC, Poluektova LY, Huang JG, Alnouti Y, Yokohira M, Arnold LL, Kabanov AV, Cohen SM, Bronich TK. Cisplatin-loaded core cross-linked micelles: comparative pharmacokinetics, antitumor activity, and toxicity in mice. Int J Nanomed. 2012;7:2557–71.
22. Gillies ER, Frechet JMJ. Development of acid-sensitive copolymer micelles for drug delivery. Pure Appl Chem. 2004;76:1295–307.
23. Sato T, Matsuda Y. Macromolecular assemblies in solution: characterization by light scattering. Polym J. 2009;41:241–51.
24. Tachibana Y, Nakazono K, Takata T. Self-assembly of macromolecular threaded systems. Supramol Chem. 2012;5:2207–23.
25. Elsabahy M, Wooley KL. Strategies toward well-defined polymer nanoparticles inspired by nature: chemistry *versus* versatility. J Polym Sci Pol Chem. 2012;50:1869–80.
26. van Nostrum CF. Covalently cross-linked amphiphilic block copolymer micelles. Soft Matter. 2011;7:3246–59.
27. Kim JO, Sahay G, Kabanov AV, Bronich TK. Polymeric micelles with ionic cores containing biodegradable cross-links for delivery of chemotherapeutic agents. Biomacromolecules. 2010;11:919–26.
28. Bae Y, Kataoka K. Intelligent polymeric micelles from functional poly(ethylene glycol)-poly(amino acid) block copolymers. Adv Drug Deliv Rev. 2009;61:768–84.
29. Lee HJ, Ponta A, Bae Y. Polymer nanoassemblies for cancer treatment and imaging. Ther Deliv. 2010;1:803–17.
30. Ponta A, Bae Y. PEG-poly(amino acid) block copolymer micelles for tunable drug release. Pharm Res. 2010;27:2330–42.
31. Eckman AM, Tsakalozou E, Kang NY, Ponta A, Bae Y. Drug release patterns and cytotoxicity of PEG-poly(aspartate) block copolymer micelles in cancer cells. Pharm Res. 2012
32. Alani AWG, Bae Y, Kwon GS. Synthesis and characterization of a micellar drug carrier for the metronomic delivery of paclitaxel. J Control Release. 2008;132:e19–20.
33. Scott D, Rohr J, Bae Y. Nanoparticulate formulations of mithramycin analogs for enhanced cytotoxicity. Int J Nanomed. 2011; 6:2757–67.
34. Le Tourneau C, Dieras V, Tresca P, Cacheux W, Paoletti X. Current challenges for the early clinical development of anticancer drugs in the era of molecularly targeted agents. Target Oncol. 2010;5:65–72.
35. Atkins JH, Gershell LJ. Selective anticancer drugs. Nat Rev Drug Discov. 2002;1:491–2.
36. Xu L, Anchordoquy T. Drug delivery trends in clinical trials and translational medicine: challenges and opportunities in the delivery of nucleic acid-based therapeutics. J Pharm Sci. 2011;100:38–52.
37. Ruenraroengsak P, Cook JM, Florence AT. Nanosystem drug targeting: facing up to complex realities. J Control Release. 2010;141:265–76.
38. Sanhai WR, Sakamoto JH, Canady R, Ferrari M. Seven challenges for nanomedicine. Nat Nanotechnol. 2008;3:242–4.
39. Grattoni A, Shen H, Fine D, Ziemys A, Gill JS, Hudson L, Hosali S, Goodall R, Liu X, Ferrari M. Nanochannel technology for constant delivery of chemotherapeutics: beyond metronomic administration. Pharm Res. 2011;28:292–300.
40. Gorn M, Habermann CR, Anige M, Thom I, Schuch G, Andritzky B, Brandl S, Burkholder I, Edler L, Hossfeld DK, Bokemeyer C, Laack E. A pilot study of docetaxel and trofosfamide as second-line 'metronomic' chemotherapy in the treatment of metastatic non-small cell lung cancer (NSCLC). Onkologie. 2008;31:185–9.
41. Jain A, Jain SK. PEGylation: an approach for drug delivery. A review. Crit Rev Ther Drug Carrier Syst. 2008;25:403–47.
42. Nel AE, Madler L, Velegol D, Xia T, Hoek EMV, Somasundaran P, Klaessig F, Castranova V, Thompson M. Understanding biophysicochemical interactions at the nano-bio interface. Nat Mater. 2009;8:543–57.
43. Vasir JK, Labhasetwar V. Quantification of the force of nanoparticle-cell membrane interactions and its influence on intracellular trafficking of nanoparticles. Biomaterials. 2008;29:4244–52.
44. Lee HJ, Bae Y. Cross-linked nanoassemblies from poly(ethylene glycol)-poly(aspartate) block copolymers as stable supramolecular templates for particulate drug delivery. Biomacromolecules. 2011;12:2686–96.
45. Bae Y, Alani AWG, Rockich NC, Lai TSZC, Kwon GS. Mixed pH-sensitive polymeric micelles for combination drug delivery. Pharm Res. 2010;27:2421–32.
46. Alani AWG, Bae Y, Rao DA, Kwon GS. Polymeric micelles for the pH-dependent controlled, continuous low dose release of paclitaxel. Biomaterials. 2010;31:1765–72.
47. Kano MR, Bae Y, Iwata C, Morishita Y, Yashiro M, Oka M, Fujii T, Komuro A, Kiyono K, Kaminishi M, Hirakawa K, Ouchi Y, Nishiyama N, Kataoka K, Miyazono K. Improvement of cancer-targeting therapy, using nanocarriers for intractable solid tumors by inhibition of TGF-β signaling. PNAS. 2007;104: 3460–5.
48. Alexis F, Pridgen E, Molnar LK, Farokhzad OC. Factors affecting the clearance and biodistribution of polymeric nanoparticles. Mol Pharm. 2008;5:505–15.
49. Zhang K, Fang H, Chen Z, Taylor John-Stephen A, Wooley Karen L. Shape effects of nanoparticles conjugated with cell-

penetrating peptides (HIV Tat PTD) on CHO cell uptake. Bioconjugate Chem. 2008;19:1880–7.
50. Decuzzi P, Gentile F, Granaldi A, Curcio A, Causa F, Indolfi C, Netti P, Ferrari M. Flow chamber analysis of size effects in the adhesion of spherical particles. Int J Nanomedicine. 2007;2:689–96.
51. Cabral H, Matsumoto Y, Mizuno K, Chen Q, Murakami M, Kimura M, Terada Y, Kano MR, Miyazono K, Uesaka M, Nishiyama N, Kataoka K. Accumulation of sub-100 nm polymeric micelles in poorly permeable tumours depends on size. Nat Nanotechnol. 2011;6:815–23.
52. Anraku Y, Kishimura A, Kobayashi A, Oba M, Kataoka K. Size-controlled long-circulating PICsome as a ruler to measure critical cut-off disposition size into normal and tumor tissues. Chem Commun. 2011;47:6054–6.
53. Untch M, Loibl S, Konecny GE, von Minckwitz G. Neoadjuvant clinical trials for the treatment of primary breast cancer: the experience of the german study groups. Curr Oncol Rep. 2012;14:27–34.
54. Falchook GS, Duvic M, Hong DS, Wheler J, Naing A, Lim J, Kurzrock R. Age-stratified phase I trial of a combination of bortezomib, gemcitabine, and liposomal doxorubicin in patients with advanced malignancies. Cancer Chemother Pharmacol. 2012; 69:1117–26.
55. Bae Y, Nishiyama N, Kataoka K. *In Vivo* antitumor activity of the folate-conjugated pH-sensitive polymeric micelle selectively releasing adriamycin in the intracellular acidic compartments. Bioconjugate Chem. 2007;18:1131–9.
56. Yokoyama M, Inoue S, Kataoka K, Yui N, Sakurai Y. Preparation of adriamycin-conjugated poly(ethylene glycol)-poly(aspartic acid) block copolymer - a new type of polymeric anticancer agent. Makromol Chem-Rapid. 1987;8:431–5.
57. Bae Y, Jang W-D, Nishiyama N, Fukushima S, Kataoka K. Multifunctional polymeric micelles with folate-mediated cancer cell targeting and pH-triggered drug releasing properties for active intracellular drug delivery. Mol Biosyst. 2005;1:242–50.
58. Duncan R. Designing polymer conjugates as lysosomotropic nanomedicines. Biochem Soc Trans. 2007;35:56–60.
59. Matsumura Y, Kataoka K. Preclinical and clinical studies of anticancer agent-incorporating polymer micelles. Cancer Sci. 2009;100:572–9.
60. Vicent MJ, Ringsdorf H, Duncan R. Polymer therapeutics: clinical applications and challenges for development. Adv Drug Deliv Rev. 2009;61:1117–20.
61. Peppas NA. Drug delivery using smart polymers: recent advances. Smart Polym. 2008:331–358
62. Satchi-Fainaro R, Duncan R, Barnes CM. Polymer therapeutics for cancer: current status and future challenges. Adv Polym Sci. 2006;193:1–65.
63. Torchilin VP. Nanocarriers. Pharm Res. 2007;24:2333–4.
64. Bae Y, Nishiyama N, Fukushima S, Koyama H, Yasuhiro M, Kataoka K. Preparation and biological characterization of polymeric micelle drug carriers with intracellular pH-triggered drug release property: tumor permeability, controlled subcellular drug distribution, and enhanced *in vivo* antitumor efficacy. Bioconjugate Chem. 2005;16:122–30.
65. Caldorera-Moore M, Guimard N, Shi L, Roy K. Designer nanoparticles: incorporating size, shape and triggered release into nanoscale drug carriers. Expert Opin Drug Deliv. 2010;7:479–95.
66. Petros RA, DeSimone JM. Strategies in the design of nanoparticles for therapeutic applications. Nat Rev Drug Discov. 2010;9:615–27.
67. Dobrovolskaia MA, Germolec DR, Weaver JL. Evaluation of nanoparticle immunotoxicity. Nat Nanotechnol. 2009;4:411–4.